JOURNAL OF AIRCRAFT
Vol. 37, No. 6, November–December 2000

Navier–Stokes Analysis of Flowfield Characteristics of an Ice-Contaminated Aircraft Wing

James Chung,* Andrew Reehorst,† Yung Choo,† Mark Potapczuk,† and John Slater‡
NASA John H. Glenn Research Center at Lewis Field, Cleveland, Ohio 44135

An analytical study was performed as part of the NASA John H. Glenn Research Center support of a National Transportation Safety Board aircraft accident investigation. The study focused on the performance degradation associated with ice contamination on the wing of a commercial turboprop-powered aircraft. Based on the results of an earlier numerical study, a prominent ridged-ice formation on the subject aircraft wing was selected for detailed flow analysis using two-dimensional, as well as three-dimensional, Navier–Stokes computations. This configuration was selected because it caused the largest lift decrease and drag increase among all of the ice shapes investigated in the earlier study. A grid sensitivity test was performed to find out the influence of grid spacing on the lift, drag, and associated angle of attack for the maximum lift $\alpha_{C_{l\max}}$. This study showed that grid resolution is important and a sensitivity analysis is an essential element of the process to assure that the final solution is independent of the grid. The two-dimensional results suggested that a severe stability and control difficulty could have occurred at a slightly higher angle of attack (AOA) than the one recorded by the flight data recorder. A decreased differential lift on the wings with respect to the normal loading for the configuration was thought to have contributed to the control upset. The analysis also indicated that this stability and control problem could have occurred whether or not natural ice shedding took place. Numerical results using an assumed three-dimensional ice shape showed an increase of the angle at which this phenomena occurred of about 4 deg. As with the two-dimensional case, the trailing-edge separation was observed but started only when the AOA was very close to the angle at which the maximum lift occurred.

Nomenclature

C_D	= three-dimensional drag coefficient
C_d	= two-dimensional drag coefficient
C_L	= three-dimensional lift coefficient
C_l	= two-dimensional lift coefficient
$C_{l\max}$	= maximum two-dimensional lift coefficient
y_1	= distance from the wing surface to the first grid point in normal direction (minimum wall spacing)
y^+	= Reynolds number based on the typical velocity and length scales for the turbulence
$\alpha_{C_{l\max}}$	= angle of attack for the maximum lift

Introduction

AIRCRAFT performance degradation due to ice contamination remains a concern within the aviation industry. Recent accidents and incidents have shown that undetected ice accretion or ineffective ice removal methods can lead to altered performance characteristics and sudden loss of stability and control, with the potential for the most severe consequences.[1] As part of a response to a request for technical assistance by the National Transportation Safety Board (NTSB), the NASA John H. Glenn Research Center Icing Branch has used simulation methods to examine the possibility of ice contamination being a contributing factor in an accident involving a commercial turboprop-powered aircraft. This examination involved tests in the Icing Research Tunnel (IRT) at NASA John H. Glenn Research Center to obtain the ice shapes that may have accreted under the flight conditions of the accident aircraft[2,3] followed by a numerical analysis effort to determine the possible performance degradation associated with those ice shapes, which is the subject of this paper. Because of higher-than-normal turbulence levels, partly due to the existence of the heat exchanger and spray bars necessary for icing cloud generation, the IRT is not considered the best facility for post-ice-accretion aeromeasurement. High-fidelity aeroperformance data are, thus, obtained from other wind-tunnel facilities. However, because of constraints of cost and of available time associated with model fabrication and for extensive wind-tunnel tests, computational fluid dynamics (CFD) was considered an alternative means of providing post-ice-accretion aeroperformance analysis.

An earlier numerical study by the authors,[2] aimed at building a foundation for flow analysis of iced airfoils, attempted to define the iced surface as closely as possible to the original geometry to make the numerical grid generation and simulation process accurate and efficient. That study showed that, for similar ice accretion times, an ice formation with a prominent ridge caused the most severe performance degradation compared to other ice shapes with only sharp bumps of similar sizes. Based on this information and the flight conditions recorded by the flight data recorder (FDR),[3] a numerical study was performed to determine if the degraded aerodynamics resulting from such an ice contamination could have contributed to the type of control upset attributed to the accident aircraft.

Approach

Ice Shape Modeling and Grid Generation

The first step in the study was the modeling of the ice shapes obtained in the IRT.[4] An ice shape with a ridge on the upper surface near the leading edge and a number of small bumps on the lower surface (Figs. 1a and 1b) was obtained in the IRT at the midsection of a vertically mounted (Fig. 1c) wing. At the centerline of this 6-ft test model, the airfoil was roughly a NACA 23015, and the chord length was about 68 in. The icing spray conditions that produced this ice shape were a median volume diameter of 20 μm, a total temperature of 26°F, an angle of attack (AOA) of 5 deg, a liquid water content of 0.8 g/m^3, and a 5-min spray time.

Among the ice shapes numerically tested, the prominent leading-edge ridged ice caused the most significant performance degradation. The height of the ridge is less than 1% of the chord (0.0074 of the chord). A glazed ice shape of this size would have been hard to

Presented as Paper 99-0375 at the 37th Aerospace Sciences Meeting, Reno, NV, 11–14 January 1999; received 20 November 1999; revision received 28 May 2000; accepted for publication 2 July 2000.

*Senior Research Associate, Institute for Computational Mechanics in Propulsion.

†Aerospace Engineer, Icing Branch.

‡Aerospace Engineer, Inlet Branch.

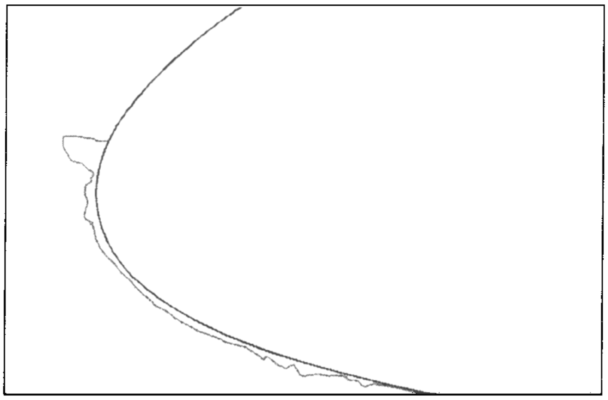

Fig. 1a Ridged-ice formation near the leading edge.

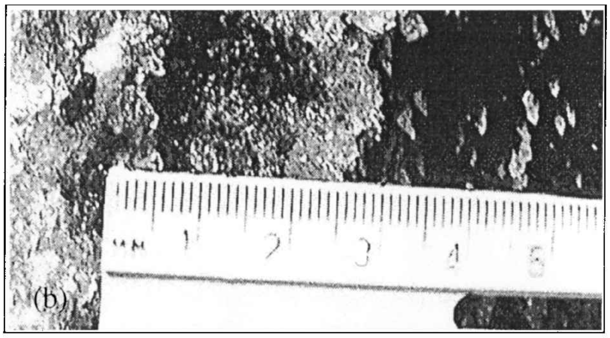

Fig. 1b Rough ice shape on the lower side of the turboprop wing, IRT experiment.

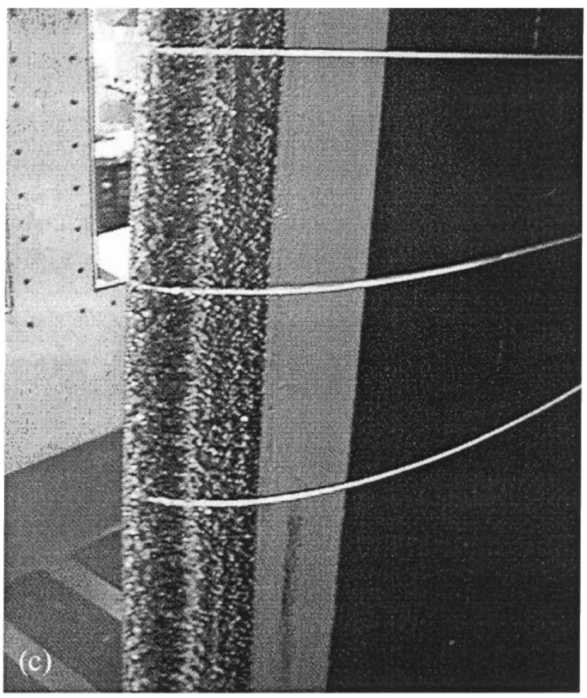

Fig. 1c Vertically mounted wing in the test section, upper surface.

see by the pilots in the cockpit. The geometry shown in Fig. 1a has several sharp corners and high curvature segments. Curve discretization and eventual generation of a quality field grid on this geometry were time consuming. A mathematical methodology for systematic surface smoothing was presented in Ref. 1. This approach was implemented in an interactive code, TURBO-GRD[5] to generate surface shapes with different smoothing levels. It constructs a smooth curve whose shape is controlled by a piecewise linear curve formed by selected discretized points. These points are called control points (CPs) because they control the shape of the curve they construct. A brief summary of this process is presented here.

1) The digitized ice shape data are first read in, and one CP is assigned to each digitized point.

2) A curve is constructed using these CPs. The discretized data points are moved onto the new smoothed curve determined by the CPs. The points are then redistributed at equally spaced intervals along the curve. The number of discretized data points on the iced segment is unchanged by this process. We will call this a baseline curve or a curve with 100% control point smoothing (CPS).

3) Using this baseline curve as a starting point, the number (or percentage) of CPs can be reduced, thus generating curves with various levels of smoothness. During this process, the shape and the number of points in the uniced areas do not change.

The current study showed that a 50% level of CPS or higher is required to represent adequately the ice shapes as measured by having marginal influence, that is, less than 5% variation, on the resulting lift and drag values. All grid generation was performed using the commercial code GRIDGEN.[6]

The two-dimensional grids used in this study for modeling the region around the iced airfoil are composed of two blocks, where the inner and outer blocks have an overlapping interface between $0.5c$ and $0.6c$, where c is the chord, from the airfoil surface. The inner block had a C-type grid with a wake cut downstream of the trailing edge and a much denser distribution of grid points than the outer block. Both blocks had downstream boundary set at $15.0c$, from the leading edge (Figs. 2a and 2b). The C-type grid was also used for the outer block with the farfield boundaries placed at a distance

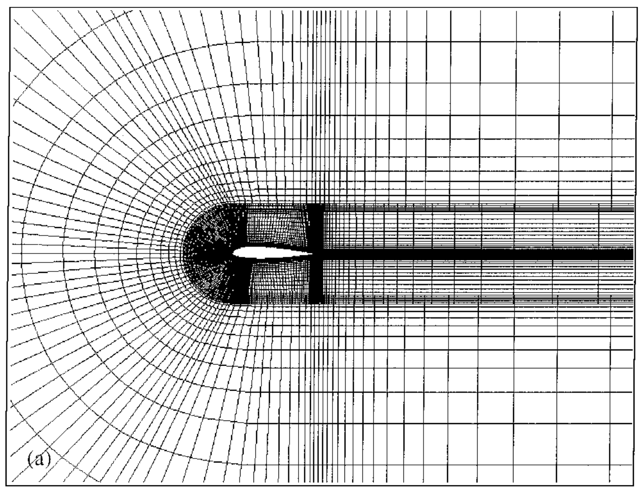

Fig. 2a Two-block grid system used for two-dimensional analysis.

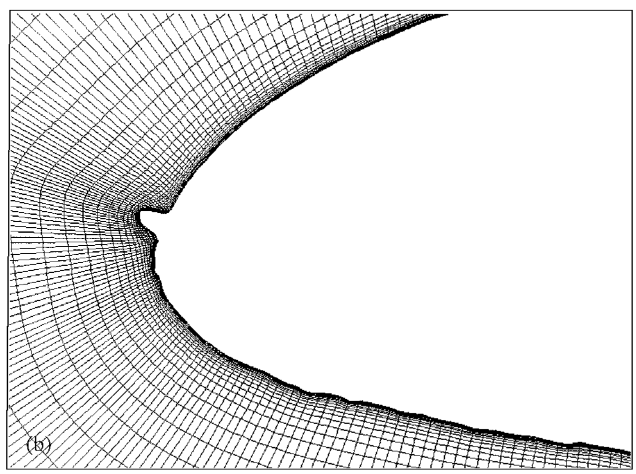

Fig. 2b Detailed grid near the ridged ice.

of 15 chord lengths from the body surface in all directions. This method of constructing two-block grids allowed for easier control of the grid generation process and better quality of the resulting grid, especially near the complex iced surfaces.

Flow Solver and Boundary Conditions

A general purpose Reynolds averaged Navier–Stokes flow analysis code, NPARC,[7] was used for the simulation. In NPARC, the Navier–Stokes equations are formulated as central-difference approximations with added artificial dissipation and are solved using an approximate-factorization scheme that results in a scalar pentadiagonal matrix for steady-state computations. Complex geometries can generally be handled with ease by the multiblock capability and modular boundary conditions. Inviscid, laminar, and turbulent flows can be simulated for two-dimensional (or axisymmetric) and three-dimensional geometries. A capability to calculate the lift and drag was added to a subroutine for this analysis. The code also has Runge–Kutta and implicit subiteration schemes for time-accurate computations. For the simulation of turbulent flows, NPARC offers algebraic, one-equation, and two-equation turbulence models. In this study, both the Spalart–Allmaras[8] and the Baldwin–Barth[9] one-equation turbulence models were used. At the far-field boundary, a non-reflecting-type boundary condition was applied.

Grid Sensitivity Test

In the absence of detailed measurement data of the pressure or velocity fields, grid sensitivity tests can be used to determine the optimum grid density. To develop the highest quality simulation of aerodynamic properties of interest, such as lift $C_{l\max}$ and drag, a series of grids (for the inner block) having different resolutions in both normal and streamwise (circumferential) directions were constructed (the outer block was fixed with the dimension of 115×20). The NPARC code was then run, using these grids, and the aerodynamic quantities of interest were compared. For this grid sensitivity test, the Spalart–Allmaras turbulence model was chosen for its known robustness in airfoil/wing calculations. Examples of the importance of grid sensitivity testing and how grid properties can affect the simulation results, especially at high AOA, may be found in Refs. 10 and 11.

The first set of grids constructed (Table 1) was used for an investigation of the normal direction sensitivity, which was followed by a study on the effect of minimum wall spacing, y_1 (Table 2), and finally by a study of the effect of packing grid points in the streamwise direction (Table 3). In Tables 1 and 3, s is the streamwise direction and n the normal direction, respectively.

Figure 3a shows that the lift values obtained using the s1n1 grid varied by over 10% from those obtained using the s1n2 grid. On the other hand, the lift values changed only 0.26–2.21% when it was refined to the level of s1n3 grid (detailed numerical values may be found in Table 4). A similar trend was observed for drag values as indicated in Fig. 3b and Table 4. This suggests that the n1s1 grid did not have a sufficient number of points to predict the maximum lift

Table 1 Grids used for normal direction sensitivity test

Grid	Dimension of the inner block	First grid off the wall	No. of points in the wake
s1n1	350×35	5.0×10^{-6}	40
s1n2	350×50	2.0×10^{-6}	40
s1n3	350×70	1.0×10^{-6}	40

Table 2 Grids used to investigate the effect of y_1

Grid	Dimension of the inner block	First grid off the wall	No. of points in the wake
w1	350×50	2.0×10^{-6}	40
w2	350×50	5.0×10^{-6}	40
w3	350×50	1.0×10^{-6}	40

Table 3 Grids used for streamwise direction sensitivity test

Grid	Dimension of the inner block	First grid off the wall	No. of points in the wake
s1n2	350×50	2.0×10^{-6}	40
s2n2	391×50	2.0×10^{-6}	45
s3n2	335×50	2.0×10^{-6}	50

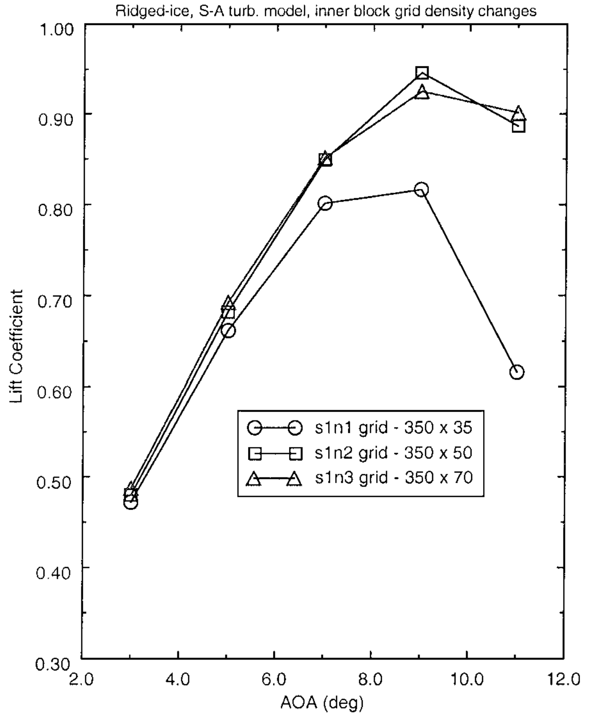

Fig. 3a Two-dimensional grid sensitivity test in normal direction: lift.

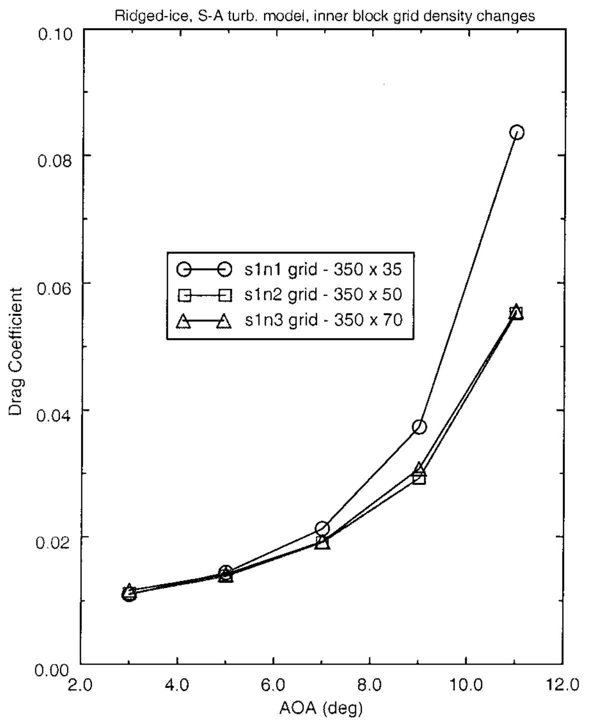

Fig. 3b Two-dimensional grid sensitivity test in normal direction: drag.

Table 4 Results of grid sensitivity test in normal direction

AOA	Grid s1n1	Grid s1n2	% Difference with respect to s1n1	Grid s1n3	% Difference with respect to s1n2
		Effect of normal direction grid spacing on the lift: S–A turbulence model			
3	0.466902E+00	0.474712E+00	1.67	0.482297E+00	1.60
5	0.656589E+00	0.677035E+00	3.17	0.687467E+00	1.55
7	0.796187E+00	0.844164E+00	6.03	0.846396E+00	0.26
9	0.811387E+00	0.940808E+00	15.95	0.920070E+00	−2.21
11	0.610636E+00	0.881574E+00	44.38	0.896499E+00	1.70
		Effect of normal direction grid spacing on the drag			
3	0.109985E−01	0.111718E−01	−1.55	0.116647E−01	4.39
5	0.144212E−01	0.138728E−01	−3.81	0.141511E−01	2.02
7	0.212905E−01	0.191165E−01	−10.10	0.192776E−01	0.84
9	0.373112E−01	0.292152E−01	−21.68	0.307334E−01	5.17
11	0.836481E−01	0.551994E−0	−34.01	0.556031E−01	0.72

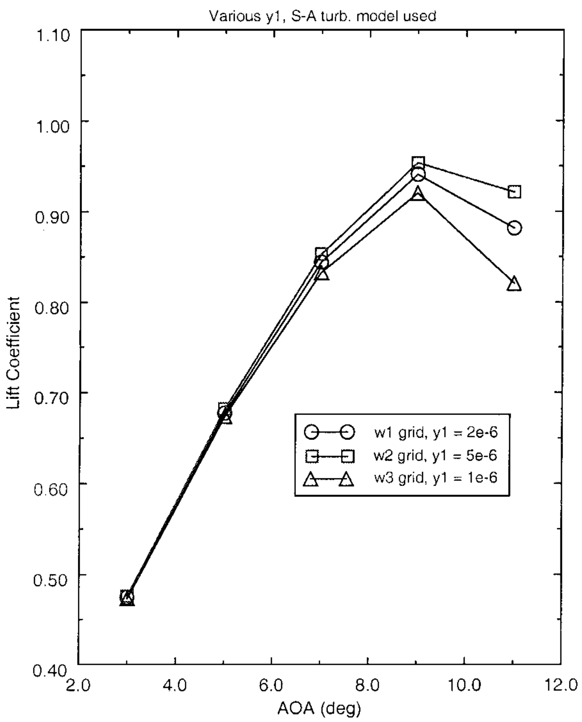

Fig. 4 Two-dimensional grid sensitivity test using minimum wall spacing.

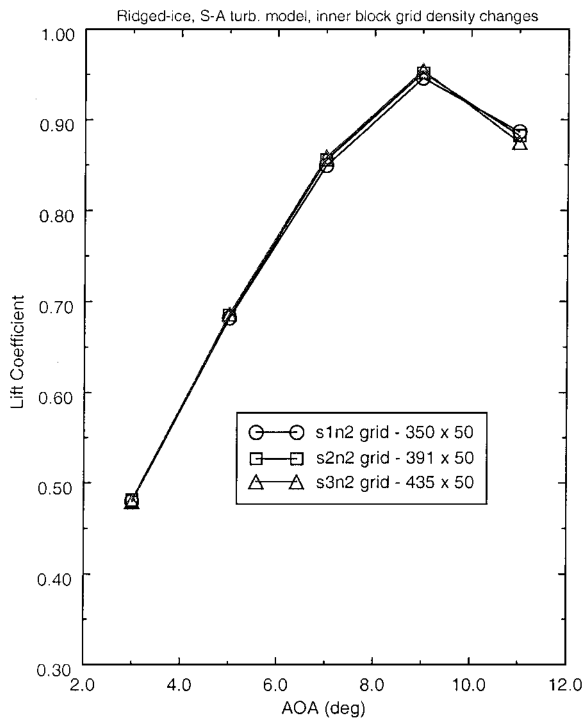

Fig. 5 Streamwise direction grid sensitivity test; two dimensions.

value and also shows that any further refinement beyond the level of the s1n2 grid was not necessary. This led to a further investigation of the effect of minimum wall spacing on aerodynamic performance parameters (see Table 2).

Another purpose of the second study was to find an appropriate value of y_1 to be used for three-dimensional grid generation that would allow efficient and fast convergence while not sacrificing accuracy. Throughout this study, the computations were performed until the L2 residual dropped at least 3–4 orders of magnitude and the lift value changed by less than 10^{-7}.

In this second step of the analysis, all aspects of the grid except the value of y_1 were fixed. Using the w1 grid as a baseline, the y_1 value was either decreased or increased to investigate the effect on the lift. Figure 4 and Table 5 show that the increase of y_1 from 2.0×10^{-6} to 5.0×10^{-6} resulted in 0.27–1.36% change in the lift value below 9-deg AOA but resulted in a 4.53% increase at 11-deg AOA. In the case of decreased y_1 (w3 grid), a similar trend was noted except that it resulted in a reduction of the lift by 0.29 ~ 2.16% up to an AOA of 9 deg and a drop of 6.91% at 11-deg AOA. An investigation of the y^+ values showed that the average value of y^+ was approximately 2.7 for the w2 grid, 1.0 for the w1 grid, and less than 1.0 for the w3 grid, respectively. This result shows that the AOA for the maximum lift was predicted for all three grids as 9 deg and that some difference existed in the computations at the 11-deg AOA. From this study, it was decided to use a y_1 of 2.0×10^{-6} for the two-dimensional studies. For the three-dimensional study, a y_1 of 5.0×10^{-6} was used for the grid generation to minimize CPU time.

To draw the final conclusion on the choice of proper grid resolution, a streamwise (circumferential) direction grid sensitivity test was performed using the three grids listed in Table 3. In this case, only the streamwise point density was changed to determine its effect on the aerodynamic performance parameters.

As Fig. 5 and Table 6 show clearly, there was less than a 1% change in the lift values regardless of the resolution. Changes in the drag were less than 1% except at the higher AOAs for the s3n2 grid (1.58% maximum). From this test, we decided to use the dimension of 350×50 with the y_1 value of 2.0×10^{-6} as the baseline.

Two-Dimensional Grids Used for the Airfoil with Ridged Ice and Aileron Deflection

According to the FDR, at the time of the NTSB-defined control upset, the left aileron deflection was 2.56 deg down and the right aileron deflection was 2.74 deg up. This configuration was intended for a right banking movement. The approximate wing AOA and Reynolds number were 7.8 deg and 10×10^6 (based on the chord), respectively. Another greater aileron deflection that occurred after

Table 5 Grid sensitivity test by varying the first spacing off the wall

AOA	Grid w1	Grid w2	% Difference with respect to w1	Grid w3	% Difference with respect to w1
Effect of y_1 spacing on the lift: S–A turbulence model					
3	0.474712*E*+00	0.476098*E*+00	0.27	0.473321*E*+00	−0.29
5	0.677035*E*+00	0.681638*E*+00	0.59	0.673610*E*+00	−0.50
7	0.844164*E*+00	0.853181*E*+00	1.07	0.832419*E*+00	−1.40
9	0.940808*E*+00	0.953617*E*+00	1.36	0.920462*E*+00	−2.16
11	0.881574*E*+00	0.921539*E*+00	4.53	0.820662*E*+00	−6.91
Effect of y_1 spacing on the drag					
3	0.111718*E*−01	0.111890*E*−01	0.18	0.112559*E*−01	0.81
5	0.138728*E*−01	0.138832*E*−01	0.07	0.139814*E*−01	0.79
7	0.191165*E*−01	0.191050*E*−01	−0.05	0.193351*E*−01	1.15
9	0.292152*E*−01	0.289606*E*−01	−0.89	0.302606*E*−01	3.56
11	0.551994*E*−01	0.526106*E*−01	−4.69	0.597563*E*−01	8.26

Table 6 Effect of streamwise direction grid refinement

AOA	Grid s1n2	Grid s2n2	% Difference with respect to s1n2	Grid s3n2	% Difference with respect to s2n2
Effect of streamwise direction refinement on the lift: S–A turbulence model					
3	0.474712*E*+00	0.475970*E*+00	0.25	0.474485*E*+00	−0.32
5	0.677035*E*+00	0.680178*E*+00	0.46	0.681312*E*+00	0.16
7	0.844164*E*+00	0.850468*E*+00	0.75	0.853843*E*+00	0.39
9	0.940808*E*+00	0.946762*E*+00	0.64	0.949348*E*+00	0.26
11	0.881574*E*+00	0.877536*E*+00	−0.47	0.869843*E*+00	−0.88
Effect of streamwise direction refinement spacing on the drag					
3	0.111718*E*−01	0.112136*E*−01	0.36	0.112155*E*−01	0.09
5	0.138728*E*−01	0.139457*E*−01	0.58	0.139903*E*−01	0.27
7	0.191165*E*−01	0.192379*E*−01	0.63	0.194336*E*−01	0.99
9	0.292152*E*−01	0.294111*E*−01	0.65	0.298083*E*−01	1.33
11	0.551994*E*−01	0.555839*E*−01	0.69	0.564566*E*−01	1.58

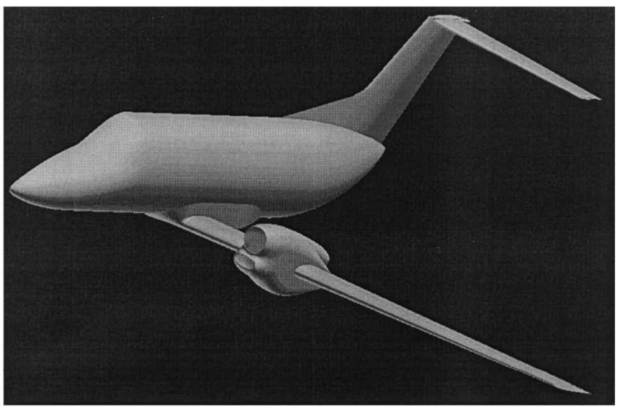

Fig. 6a Turboprop aircraft used for the numerical analysis in a shaded mode.

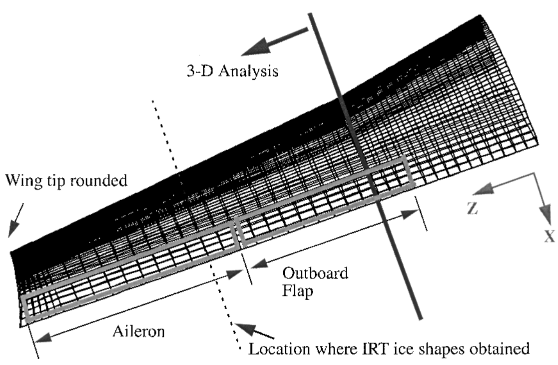

Fig. 6b Three-dimensional wing modeling showing the area of numerical analysis.

the defined control upset was 7.94-deg aileron down on the left wing (LW) and 8.26 deg up on the right wing (RW).

Four grids for the airfoil with ridged-ice accretion, reflecting these four different angles of aileron deflection, were generated using the guidelines developed from the grid sensitivity tests. More grid points were used near the aileron in the streamwise direction over the grids used in the sensitivity study. Another set of four grids for airfoils without ice but having the same aileron deflection angles were also generated for comparison to the iced airfoils.

Three-Dimensional Grid Generation

Initial graphics exchange specifications type surface data of the turboprop aircraft are shown in a shaded mode in Fig. 6a. The geometry data are obtained from the manufacturer, and some assumptions were made to generate the grids for both iced and uniced wings.

A number of assumptions are worth noting: First, the available data did not have information about the wing tip geometry. Figures 7c and 7d show the approximated wing tip used in the analysis. Second, as shown in Fig. 6b, only the outboard section of the wing (approximately 5.4 m in the spanwise direction) was used for the current analysis to reduce the time required to model the complicated engine block primarily due to a tight schedule for the project. Another reason for this simplification was uncertainty about the ice shapes on the wing sections near the propeller. Therefore, the three-dimensional computations were focused on checking the flow quality around the aileron and wing tip. Third, the downward deflected aileron on the left wing (only 2.56-deg deflection angle) was modeled as having no gap with the wing surface in the spanwise direction. This was accomplished by creating a smoothly connected surface shape shown in Fig. 7e (see also Fig. 7c). The idea behind this was that the existence of a fence on the real aircraft between the aileron and the outboard flap next to it would have prevented any spanwise flow. Fourth, for the modeling of an assumed three-dimensional ice shape, the absolute height and the shape of the ridged ice on the upper surface and of the bumps on the lower

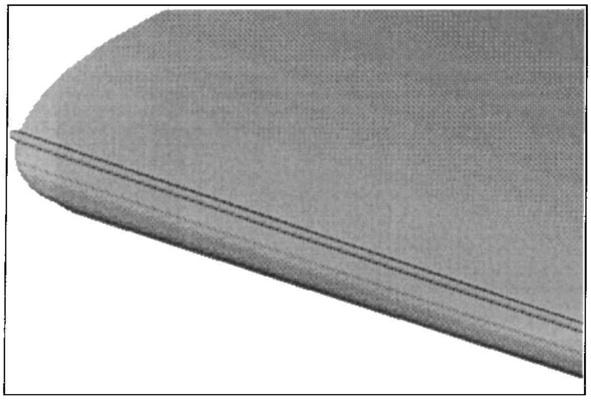

Fig. 7a Ice shape at the leading edge of the wing.

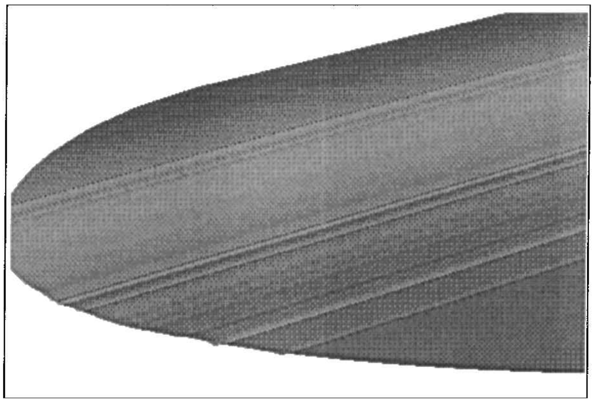

Fig. 7b Ice shape modeling on the lower surface.

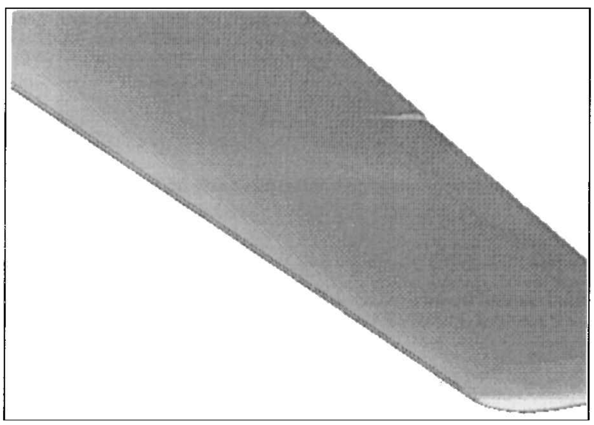

Fig. 7c Aileron and wing tip.

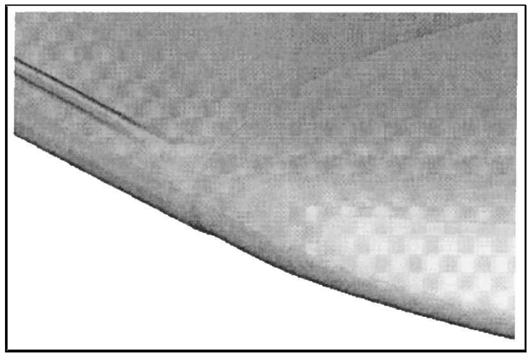

Fig. 7d Tapering ice shape near the simulated wing tip.

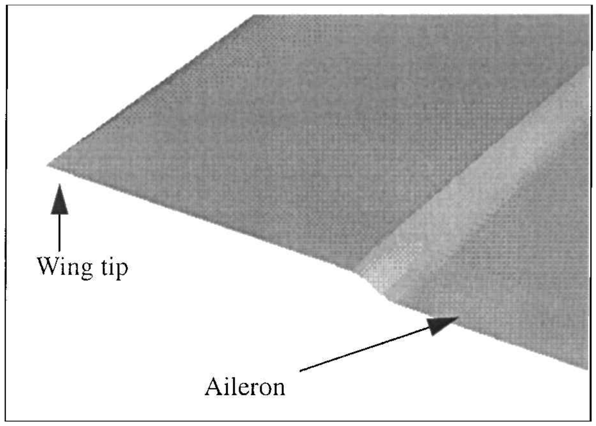

Fig. 7e Modeling of the aileron at 2.56 deg down.

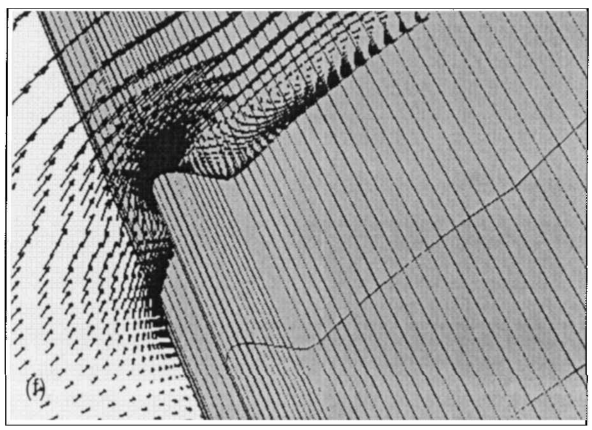

Fig. 7f Grid system at the ridged ice and the separation behind it.

surface were kept constant (Figs. 7a and 7b). They were projected in both spanwise directions from the location where the ice shape data were taken in the IRT (see Fig. 6b). Because the wing did not have a large sweep angle and the maximum thickness was larger near the root, the root area had a lower collection efficiency. Thus, it was considered to be a plausible assumption to use a constant cross section ice shape and to taper it smoothly near the wing tip (Fig. 7d).

Figure 7f shows an example of grid lines around the ridge and a typical velocity profile showing separation behind it. Based on the preceding assumptions, three-dimensional grids consisting of approximately 4×10^5 and 1×10^6 grid points in a single-block format were generated for the clean (uncontaminated) and iced wings with an aileron deflection angle of 2.56 deg. The symmetry plane was located at $z = 4.5$ m ($z = 0$ being the fuselage centerline), and the spanwise location of the aileron was between $z = 6.3$ and 9.6 m. The three-dimensional computational results were compared to the two-dimensional results at the $z = 6.59$ m location where the two-dimensional IRT ice shape was taken.

Discussion of Results

Two-Dimensional Flow Analysis

Aileron Deflection 1 (2.56 Down LW, 2.74 Up RW)

Figures 8a–9b show the lift and drag coefficients vs AOA obtained by steady-state computations using two different one-equation turbulence models, Spalart–Allmaras (S–A).[8] and Baldwin–Barth (B–B).[9] This calculation was performed to investigate differences in the numerical prediction resulting from the application of these two models. Both Figs. 8a (S–A) and 9a (B–B) show that the ice caused a slight lift decrease at low AOAs and a further significant decrease at higher angles.

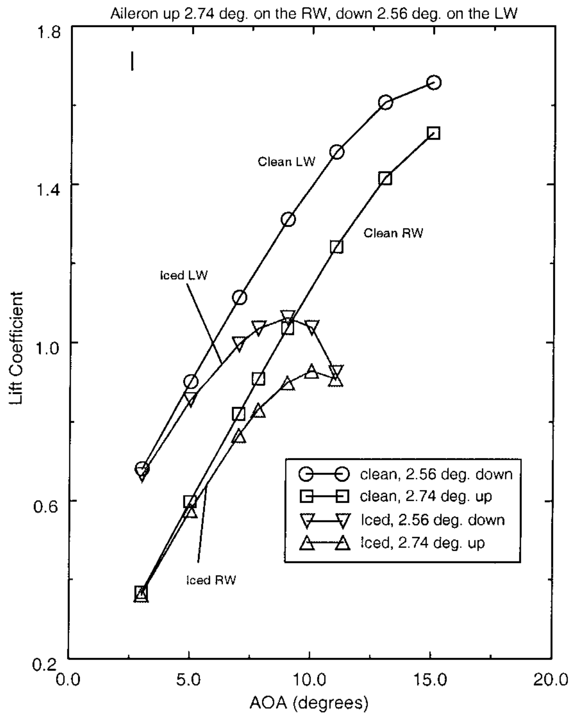

Fig. 8a Lift comparison for airfoil with ridged ice.

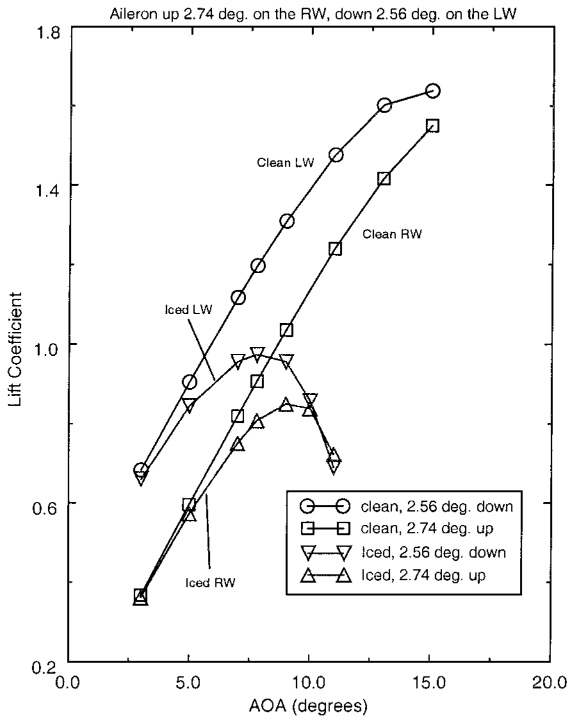

Fig. 9a Lift comparison for airfoil with ridged ice.

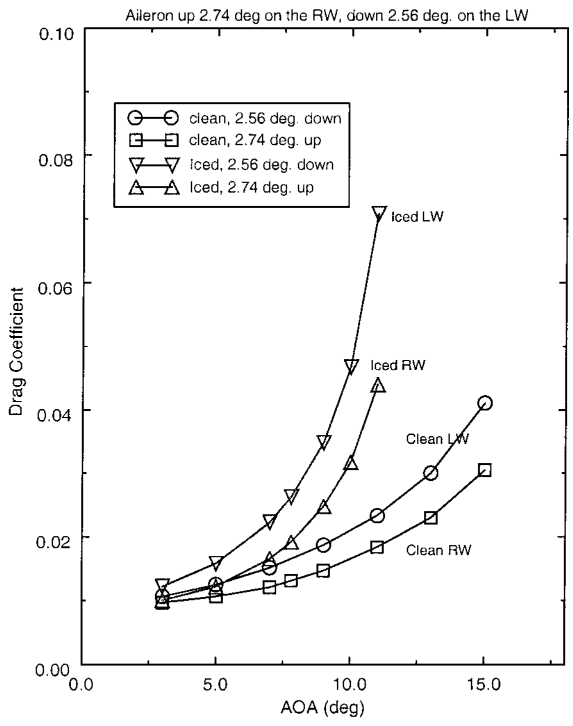

Fig. 8b Drag comparison for airfoil with ridged ice; S–A turbulence model used for the two-dimensional computation.

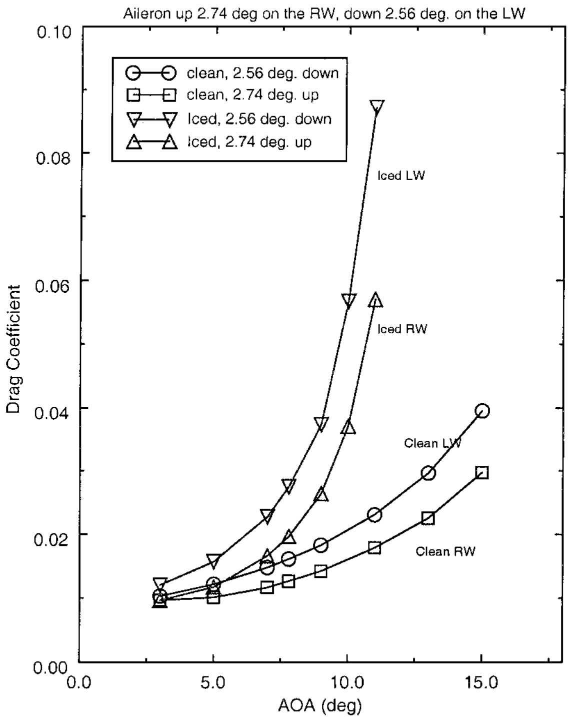

Fig. 9b Drag comparison for airfoil with ridged ice; B–B turbulence model used for the two-dimensional computation.

The open circles represent lift values for the uncontaminated LW with 2.56-deg aileron down and the squares represent those of uncontaminated RW with 2.74-deg aileron up. We assume that no ice shedding occurred on any of the wings. The lift was computed every 2 deg between 3 and 15 deg for the uniced wings. Without the ice, as the lift curves show, the airplane would not have had any problem banking to the right with the higher lift on the LW. The iced-wing computations were done for AOA of 3, 5, 7, 7.8, 9, 10, and 11 deg (7.8 deg was the AOA where the control problem occurred according to the FDR).

A close examination of the lift change on the iced LW predicted by the S–A turbulence model in Fig. 8a shows that the peak value occurred around 9 deg. The maximum lift was predicted to occur at a slightly lower AOA [7.8 deg (Fig. 9a)], when the B–B model was used. The maximum lift on the iced RW occurred at approximately 10 deg for the S–A model (Fig. 8a) and 9 deg for the B–B model (Fig. 9a). Also noticeable from the two graphs is that a reversal of lift differential occurs at around 11 and 10.5 deg, respectively, and it could have caused difficulty in aileron control.

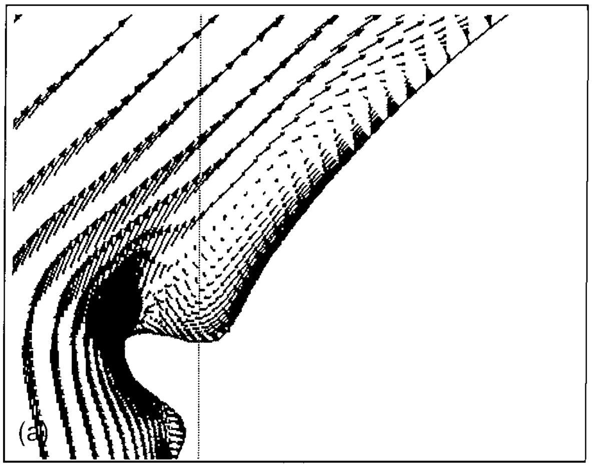

Fig. 10a Separation aft of the ridged ice.

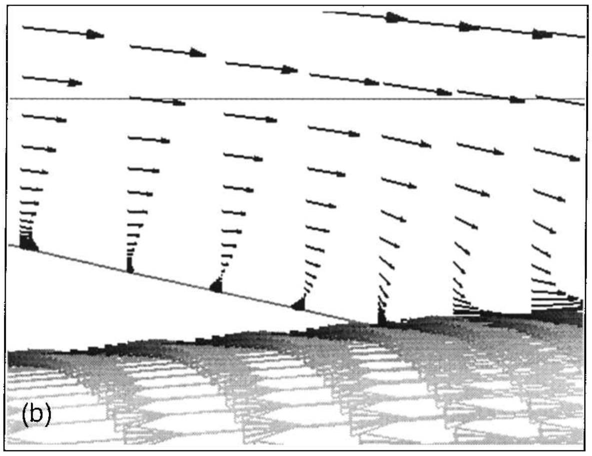

Fig. 10b Trailing-edge separation at AOA = 7: two-dimensional.

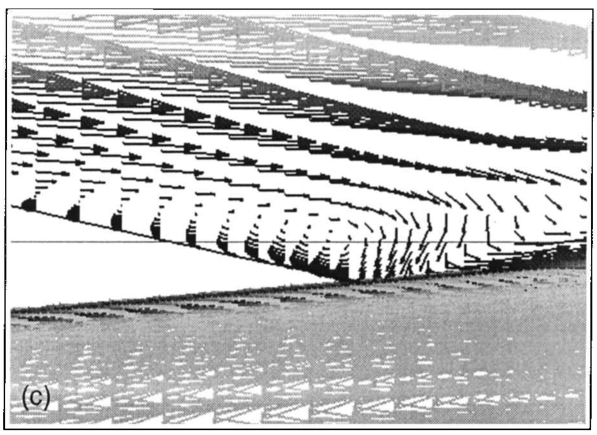

Fig. 10c Increased trailing-edge separation at AOA = 9: two-dimensional.

Now, if we consider the possibility of ice completely shedding off the RW, as was indicated by the experiment in the IRT,[4] the reversal of the lift values could occur at a lower AOA. In this case, 9 (S–A) or 8 (B–B) deg would be the approximate angles where the reversal would have happened. These are angles fairly close to those recorded by the FDR. Computation for higher than 11-deg AOA was not attempted because of the expected unsteady nature of the flow.

Figures 8b and 9b show the drag coefficient prediction using the two turbulence models. They indicate a considerable increase in the drag but show no crossover of the drag values for the iced wings. Figures 8b and 9b both indicate that the LW showed consistently higher drag values than the RW. This supports the FDR record that there was a tendency for yaw in the counterclockwise direction before the accident happened. A little closer examination of the four graphs also show that the S–A model predicted slightly higher lift and lower drag values than the B–B model. Though different from the current study, a previous computational study[12] using these

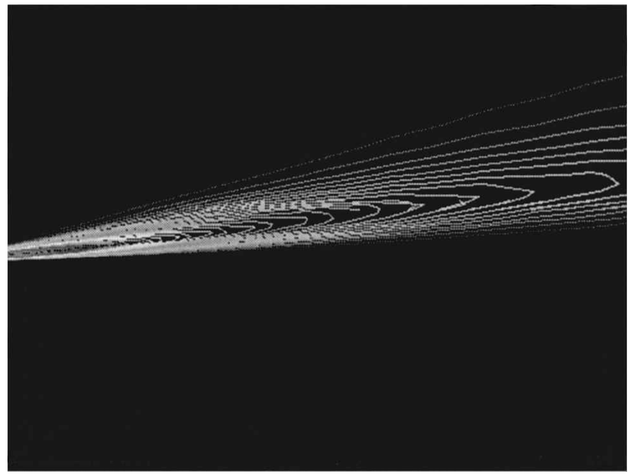

Fig. 11 Turbulent viscosity contour: AOA = 9 deg, two-dimensional.

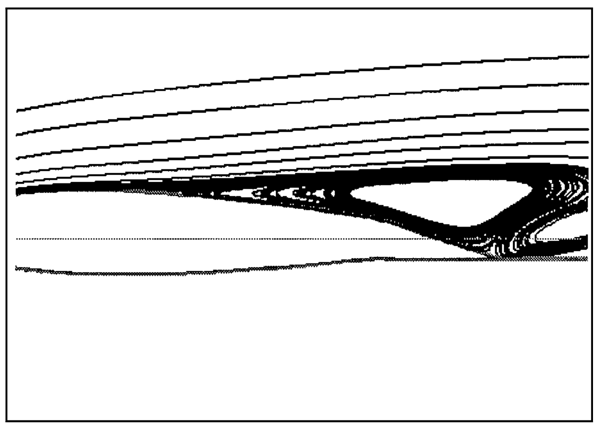

Fig. 12 Large separation near the trailing edge at AOA = 10 deg for 7.94-deg downward aileron deflection; two-dimensional.

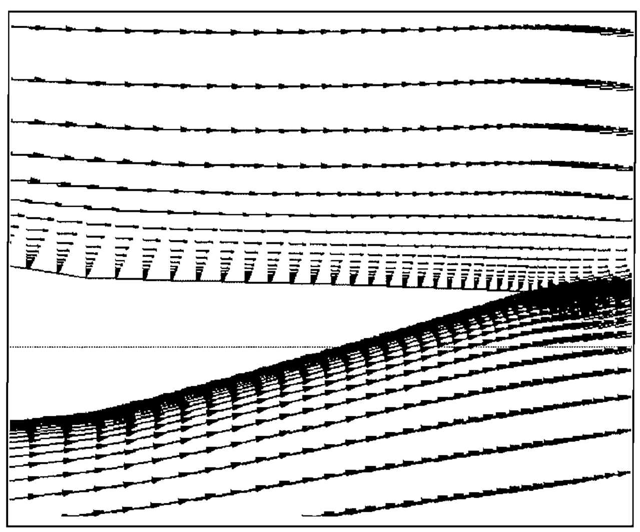

Fig. 13 Velocity profile of the trailing edge of aileron deflected 8.26 deg upward at AOA = 10 deg; two-dimensional.

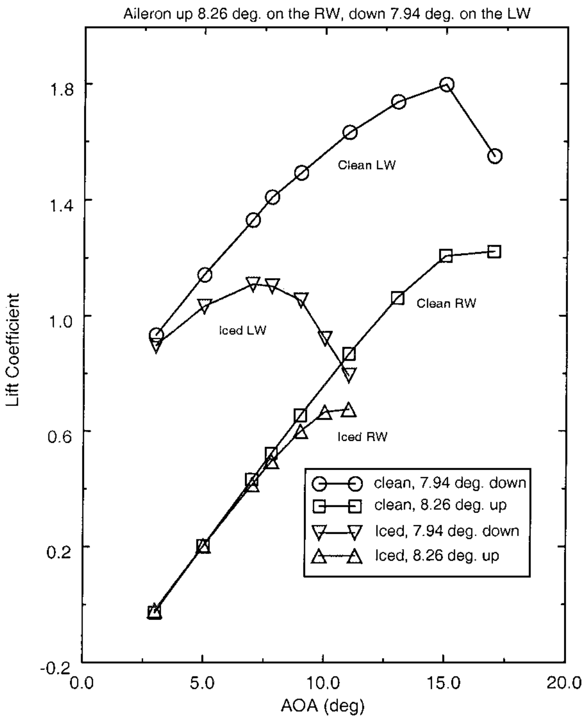

Fig. 14a Lift comparison for airfoil with ridged ice for higher-angle aileron deflection.

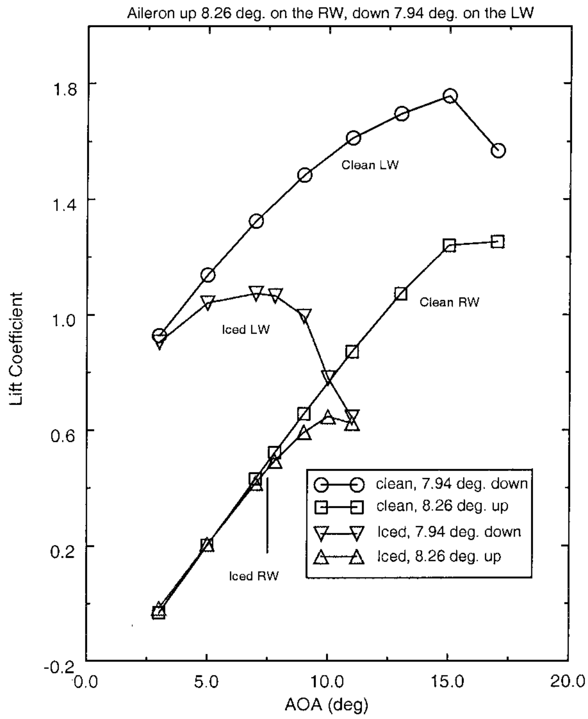

Fig. 15a Lift comparison for airfoil with ridged ice for higher-angle aileron deflection.

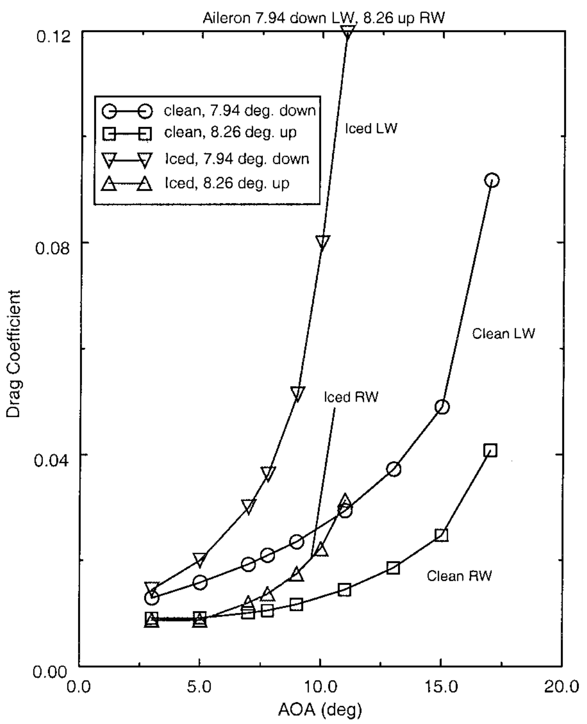

Fig. 14b Drag comparison for airfoil with ridged ice for higher-angle aileron deflection; S–A turbulence model used for the two-dimensional computation.

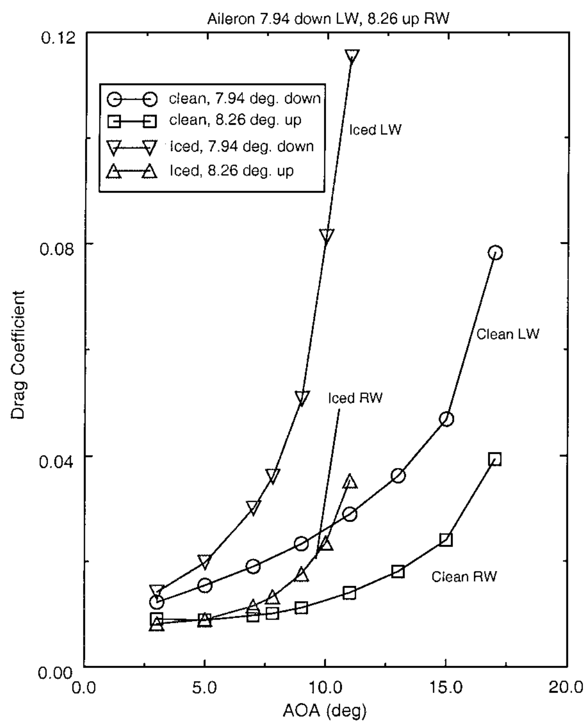

Fig. 15b Drag comparison for airfoil with ridged ice for higher angle aileron deflection; B–B turbulence model used for the two-dimensional computation.

turbulence models suggests that difference in the spreading rates (or amount of mixing) in the wake regions could be a contributing factor to these differences. Figures 10a–10c show the leading-edge and trailing-edge separation predicted by the S–A turbulence model. The trailing-edge separation starts at an AOA of 7 deg, and this separation region grows as the AOA increases. When the AOA reaches 9 deg, the trailing-edge separation covers almost 70% of the upper surface. Figure 11 shows the turbulent viscosity contour at the 9-deg AOA.

Aileron Deflection 2 (Down 7.94 LW, Up 8.26 RW)

A higher angle aileron input was applied to attempt to bank to the right after the defined control upset. This condition was also simulated using the two-dimensional Navier–Stokes analysis procedure (Figs. 12–15). Unlike the preceding lower aileron angle setting, the crossover of lift was not observed for the AOA analyzed, but a considerable decrease of the lift differential between the S–A and B–B turbulence model was predicted (Figs. 14a and 15a). As expected, the lift differential between the LH and RH wings is larger with the increased aileron deflection, and the data suggest a reversal of the lift differential at an AOA greater than that investigated. However, under aileron setting 2, the effectiveness of the aileron might have been significantly reduced at slightly lower AOA due to the decreased lift differential, which raised the possibility of the control dilemma. As occurred with setting 1, shedding of the ice from the RW would have still caused the lift reversal, at a slightly higher AOA of 10 deg. The S–A turbulence model predicted higher lift and lower drag values than the B–B model with the exception of the 11-deg AOA case. At this angle, the S–A model predicted a higher value for both lift and drag than the B–B model.

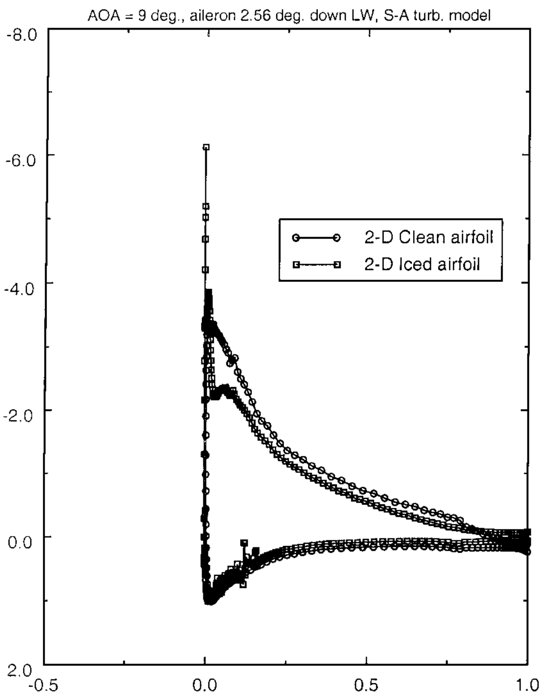

Fig. 16a Two-dimensional pressure coefficient comparison between clean and iced airfoils.

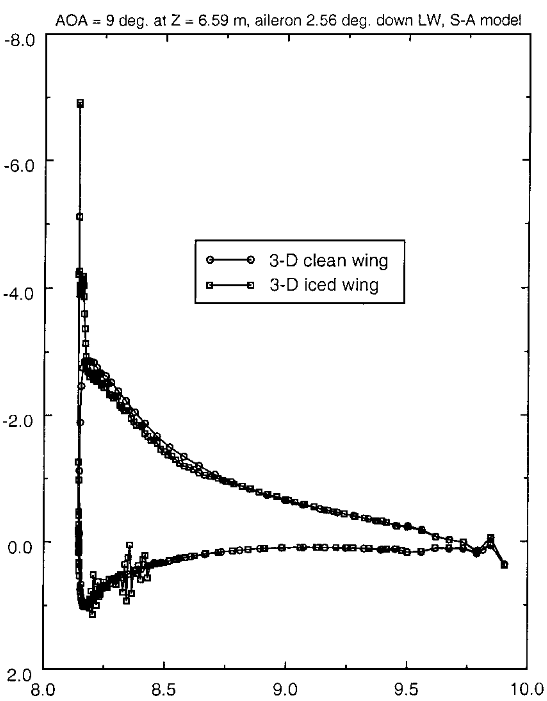

Fig. 16b Three-dimensional pressure coefficient comparison between clean and iced airfoils.

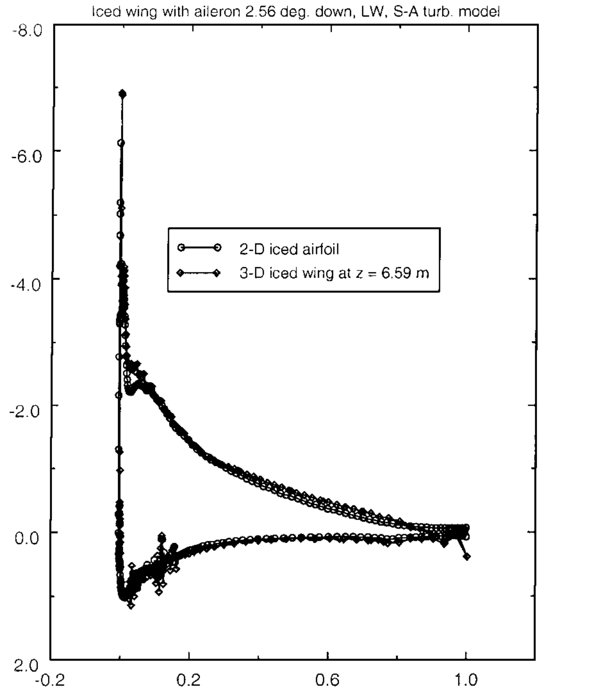

Fig. 16c Two- and three-dimensional pressure coefficient comparison at AOA = 9 deg.

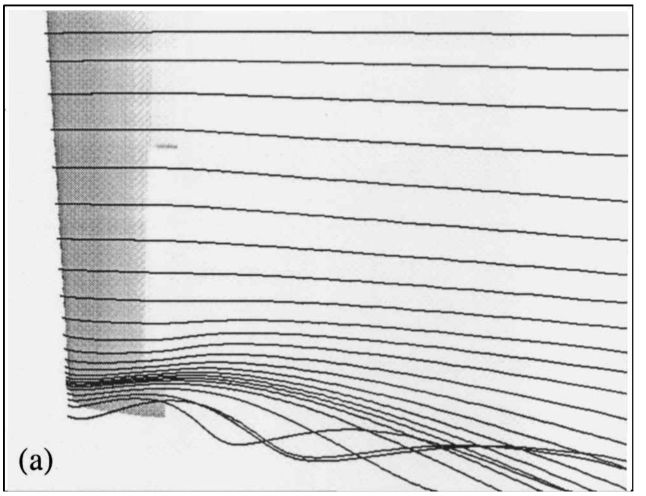

Fig. 17a Rake profile for three-dimensional wing at AOA = 13 deg.

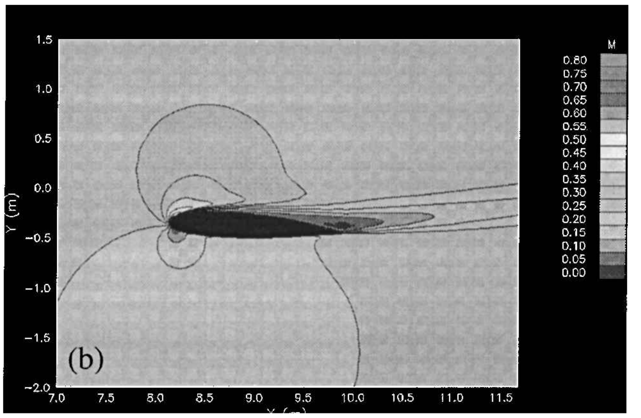

Fig. 17b Mach contour at AOA = 13 deg.

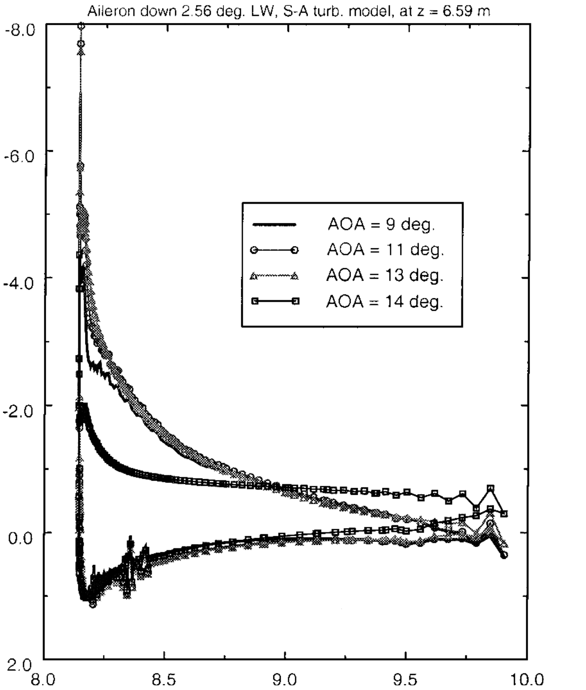

Fig. 18 C_p **change at various AOAs for three-dimensional iced wing.**

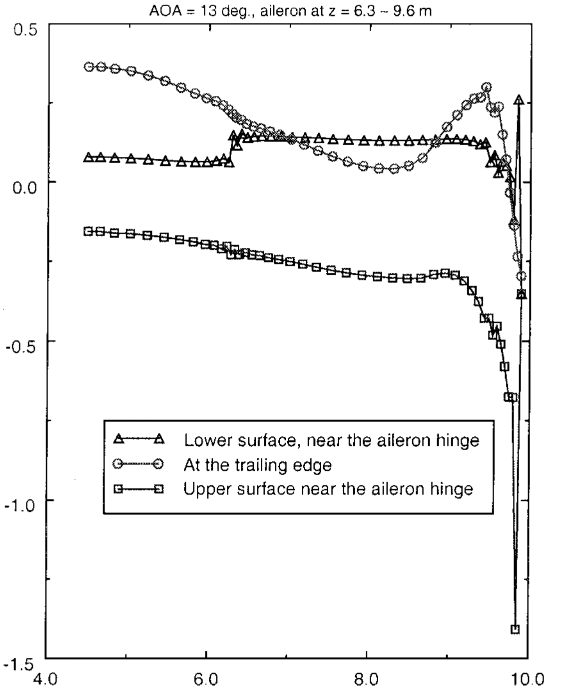

Fig. 19a C_p **distribution in spanwise direction for three-dimensional iced wing at AOA = 13 deg.**

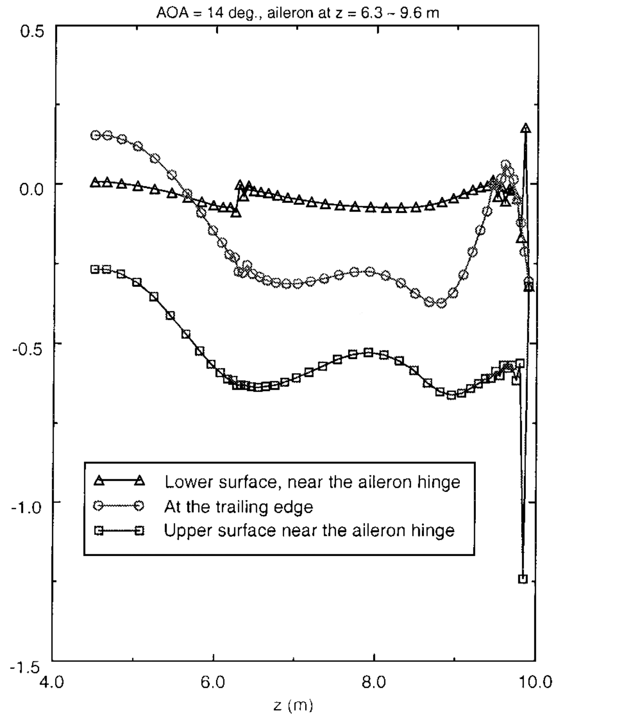

Fig. 19b C_p **distribution in spanwise direction for three-dimensional iced wing at AOA = 14 deg.**

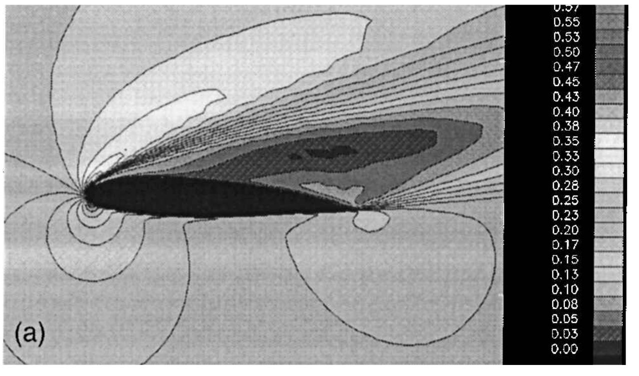

Fig. 20a Mach contour at AOA = 14 deg.

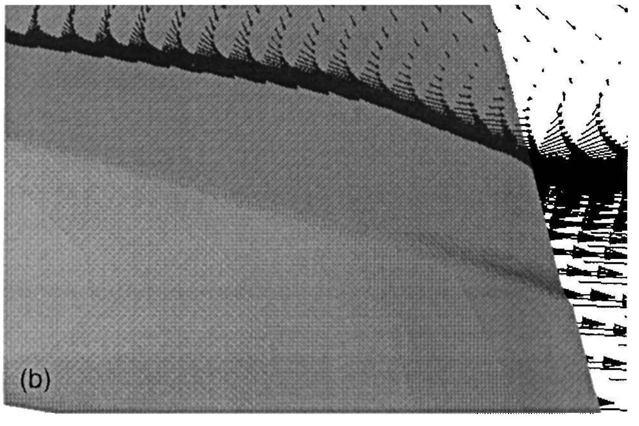

Fig. 20b Trailing-edge separation near the wing tip.

Three-Dimensional Flow Analysis

Because of the time requirements for the calculations, the three-dimensional analysis was limited to only one downward aileron deflection angle of 2.56 deg on the LW for both iced and clean cases. This calculation was performed to investigate whether there were any three-dimensional effects that altered the two-dimensional flow characteristics. The S–A model was used for all three-dimensional computations, and the results were compared to those of the two-dimensional computations using the same S–A model.

The three-dimensional computation showed that the $\alpha_{C_{l\max}}$ occurs at about 13 deg, approximately 4 deg higher than the two-dimensional case. At 9-deg AOA, where the two-dimensional calculation showed considerable change in the pressure coefficient plot on the upper surface (Fig. 16a), the three-dimensional calculation showed little difference between the clean and the iced wings (Fig. 16b). The comparison of the two-dimensional and three-dimensional pressure coefficients shows some differences just aft of the ridge and at about 0.6 x/c on the upper surface (Fig. 16c). The rake profile and Mach contour plots from the three-dimensional analysis at an AOA of 13 deg (Figs. 17a and 17b) indicate that no

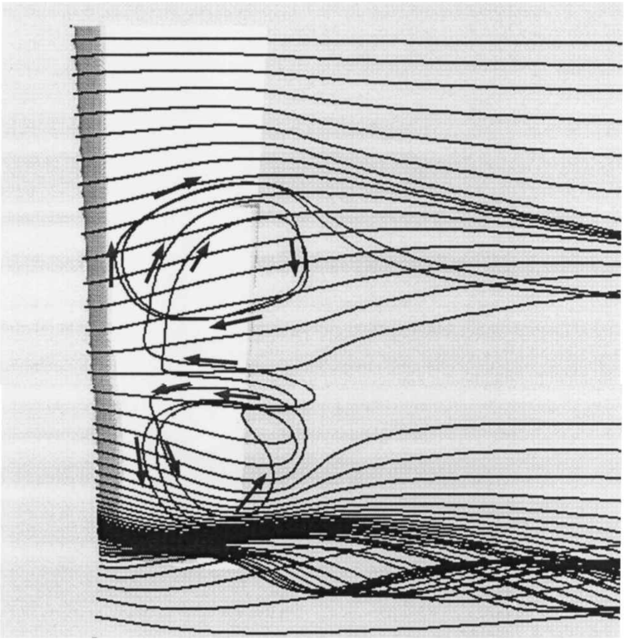

Fig. 21 Circular flow pattern on the upper surface of the iced wing appearing at AOA = 14 deg.

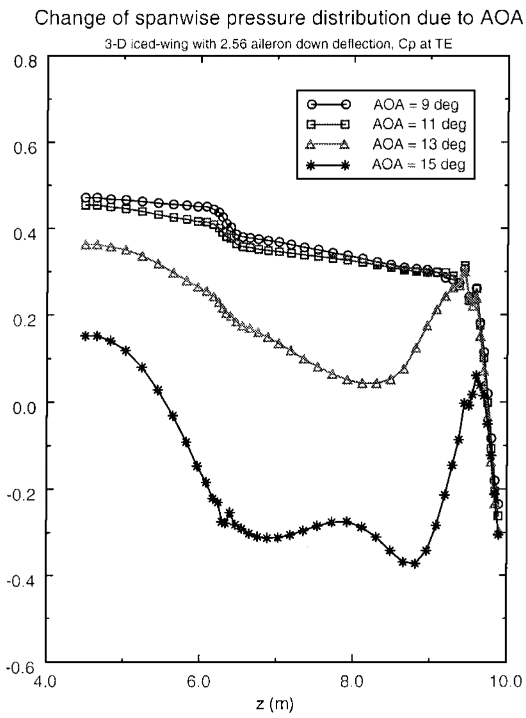

Fig. 22 Change of spanwise pressure distribution at various angles.

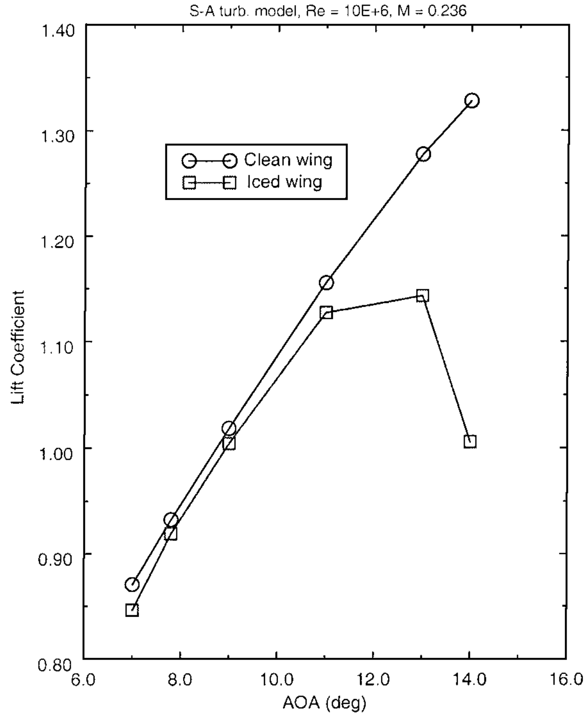

Fig. 23 Lift comparison for the three-dimensional wing.

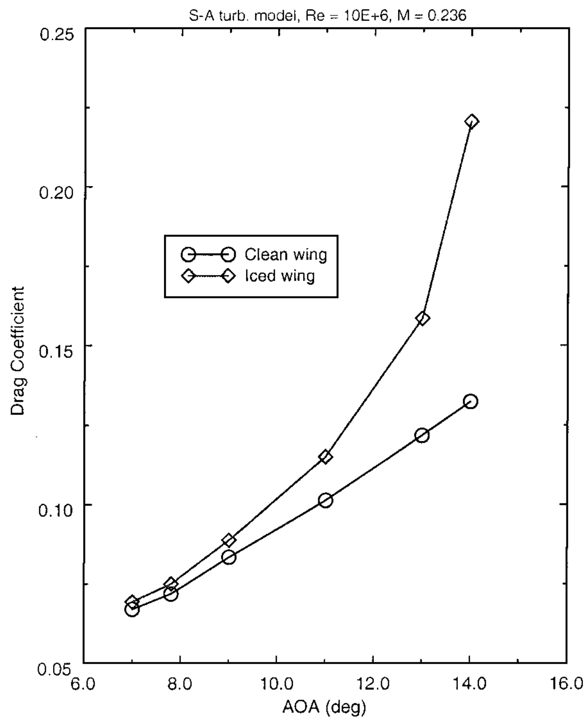

Fig. 24 Drag comparison for the three-dimensional wing.

large-scale separation occurs near the trailing-edge on the upper surface. At 14-deg AOA though, a trailing-edge separation starts, as shown in the next series of graphs showing pressure coefficient (Fig. 18), spanwise variation of the pressure along lines parallel to the trailing edge (Figs. 19a and 19b), Mach contour (Fig. 20a), and velocity profile (Fig. 20b). The rake profile at 14-deg AOA (Fig. 21) shows a large separation region on the upper surface as well as circular motion of the fluid parallel to the wing surface. This occurs near the spanwise region where the aileron was deflected. The change of spanwise pressure distribution shown in Fig. 22 indicates that a small-scale trailing-edge separation started at an AOA of 13 deg and intensified at 14-deg AOA. The differences in the lift and in the drag between the clean three-dimensional wing and the iced three-dimensional wing are shown in Figs. 23 and 24. The three-dimensional lift and drag are defined as

$$C_L = L/q_\infty S, \qquad C_D = D/q_\infty S$$

where q_∞ is dynamic pressure and S is a reference area (wing span × mean chord) and L and D are total lift and drag of the entire wing, respectively. The causes of the difference between the two- and three-dimensional computations are probably due to one or more of the following: 1) finite wing effects,[13] 2) relatively poor resolution of the three-dimensional grids, and 3) proportionally smaller ridge height at the inboard section of the wing, which may have affected the trailing-edge separation at the lower AOA. Because of the three-dimensional nature of the flow, this could affect the flow in the outboard section as well. A fourth cause is that the smooth end plating of the deflected aileron could affect possible aileron loading.

Conclusions

The purpose of this study was to perform a post-ice-accretion CFD analysis of the contaminated airfoil/wing surfaces of a turboprop aircraft under the reconstructed icing conditions from an accident. This analysis was performed to obtain some qualitative trends and to provide insight into the aerodynamics that may have led to a control upset. The grid sensitivity tests that preceded the numerical simulation showed that the prediction of accurate lift and drag values as well as AOA of maximum lift can be affected by the grid resolution. The two-dimensional analysis indicated that the control upset could have occurred with or without the complete ice shedding at or slightly higher than the AOA recorded by the FDR. The performance degradation was observed to be a result of a combination of trailing- and leading-edge separation. In the case of three-dimensional analysis, the trailing-edge separation was observed to start near the maximum-lift point. The three-dimensional results also showed that the maximum lift occurred 4 deg later than the two-dimensional case. More work is needed in three-dimensional ice shape modeling and in grid refinement to understand the differences between the two-dimensional and three-dimensional results.

References

[1]"National Transportation Safety Board Aviation Accident Report, In Flight Icing Encounter and Uncontrolled Collision with Terrain, Comair Flight 3272, Embraer EMB-120T, N265CA Monroe, Michigan, January 9, 1997," National Transportation Safety Board, NTSB Accident DCA97MA017, Nov. 1998.

[2]Chung, J., Reehorst, A., Choo, Y., and Potapczuk, M., "Effect of Airfoil Ice Shape Smoothing on the Aerodynamic Performances," AIAA Paper 98-3242, July 1998.

[3]"The Group Chairman's Aircraft Performance Study," National Transportation Safety Board, NTSB Accident DCA97MA017, Sept. 1998.

[4]Reehorst, A., Chung, J., Potapczuk, M., Choo, Y., Wright, W., and Langhals, T., "Study of Icing Effects on Performance and Controllability of an Accident Aircraft," *Journal of Aircraft*, Vol. 37, No. 2, 2000, pp. 253–259.

[5]Choo, Y., Slater, J., Henderson, T., Bidwell, C., Braun, D., and Chung, J., "User Manual for Beta Version of Turbo-GRD—A Software System for Interactive Two-Dimensional Boundary/Field Grid Generation, Modification, and Refinement," NASA TM-1998-206631, Oct. 1998.

[6]Chawner, J., and Steinbrenner, J., "Automatic Grid Generation Using GRIDGEN," *Surface Modeling, Grid Generation, and Related Issues in CFD Solutions*, NASA, CP-3291, May 1995.

[7]"NPARC Version 3.0 User's Manual," NPARC Alliance, Sept. 1996.

[8]Spalart, P., and Allmaras, S., "A One-Equation Turbulence Model for Aerodynamic Flows," AIAA Paper 92-0439, Jan. 1992.

[9]Baldwin, B., and Barth, T., "A One-Equation Turbulence Transport Model for High Reynolds Number Wall-Bounded Flows," AIAA Paper 91-0610, Jan. 1991.

[10]Rogers, S., "Progress in High-Lift Aerodynamic Calculations," AIAA Paper 93-0194, Jan. 1993.

[11]Anderson, W., "Navier–Stokes Computations and Experimental Comparisons for Multi-Element Airfoil Configurations," AIAA Paper 93-0645, Jan. 1993.

[12]Rogers, S., Menter, F., Durbin, P., and Mansour, N., "A Comparison of Turbulence Models in Computing Multi-Element Airfoil Flows," AIAA Paper 94-0291, Jan. 1994.

[13]Polhamus, E., "A Survey of Reynolds Number and Wing Geometry Effects on Lift Characteristics in the Low Speed Stall Region," NASA CR 4745, June 1996.